Published online June 9, 2004

3136–3147 *Nucleic Acids Research, 2004, Vol. 32, No. 10*
DOI: 10.1093/nar/gkh633

Recognition of DNA by ω protein from the broad-host range *Streptococcus pyogenes* plasmid pSM19035: analysis of binding to operator DNA with one to four heptad repeats

Ana B. de la Hoz, Florencia Pratto, Rolf Misselwitz[1], Christian Speck[2], Wilhelm Weihofen[3], Karin Welfle[1], Wolfram Saenger[3], Heinz Welfle[1] and Juan C. Alonso*

Departamento de Biotecnología Microbiana, Centro Nacional de Biotecnología, CSIC, 28049 Madrid, Spain, [1]Max-Delbrück-Centrum für Molekulare Medizin, 13092 Berlin, Germany, [2]Max-Planck-Institut für Molekulare Genetik, 14195 Berlin, Germany and [3]Institut für Kristallographie, Freie Universität Berlin, 14195 Berlin, Germany

Received February 19, 2004; Revised April 28, 2004; Accepted May 13, 2004

ABSTRACT

pSM19035-encoded ω protein forms a dimer (ω_2) that binds to a set of 7-bp repeats with sequence 5′-NATCACN-3′. Upon binding to its cognate sites, ω_2 regulates transcription of genes required for copy number control and stable inheritance of plasmids, and promotes accurate plasmid segregation. Protein ω_2 binds poorly to one heptad but the affinity to DNA increases with two and more unspaced heptads in direct or inverted orientation. DNA titration of increasing numbers of heptads with ω_2, monitored by circular dichroism measurements, indicates the binding of one ω_2 to one heptad (ω_2:heptad stoichiometry of 1:1). Spacing of two directly or inversely oriented heptads by 1 to 7 bp reduces the affinity of the protein for its cognate target site. The binding affinity of ω_2 for two directly repeated heptads was severely reduced if one of the base pairs of the core 5′-ATCAC-3′ sequence of one of the heptads was individually substituted by any other base pair. Hydroxyl radical footprinting shows a protection pattern at the 5′-ATCAC-3′ core. These data suggest that each heptad defines an operator half-site and that tight binding of the symmetric ω_2 to the central 5′-TCA-3′ core of symmetric or asymmetric targets (differently oriented heptads) is probably achieved by structural changes of DNA and/or protein or both.

INTRODUCTION

Gene regulation in prokaryotes is achieved largely by proteins, having predominantly helix–turn–helix (HTH) DNA binding motifs, and interacting specifically with palindromic DNA sequences to repress or activate expression of associated genes or groups of genes (1). Recognition of arrays of short direct DNA repeats by specific transcriptional regulators is rare in bacteria (2–5). The ribbon–helix–helix (RHH) or $(\beta\alpha\alpha)_2$ proteins are a growing family of DNA binding proteins, of which many have been studied by X-ray crystallography and NMR spectroscopy (6–12). Among the characteristics associated with the DNA-binding domain of $(\beta\alpha\alpha)_2$ proteins are two-stranded antiparallel β-sheets that make sequence-specific contacts with the major groove of DNA, and several residues of the second α-helix (αB) interact with phosphates of the DNA backbone. Most RHH proteins, which are symmetric dimers, bind as tetramers, or higher order oligomers, to operator sequences containing two or more binding sites that are usually arranged as inverted (Arc, CopG) or direct (MetJ) repeats for each dimeric DNA-binding protein domain (6,7,9). The MetJ interacts symmetrically with its directly repeated cognate site, whereas the Arc and CopG proteins interact asymmetrically with their palindromic targets (6,7,9).

The *Streptococcus pyogenes* pSM19035-encoded ω_2 protein, which belongs to a family of RHH DNA-binding proteins, binds to upstream promoter regions of genes involved in copy number control (*Pcop*S), partition (*P*δ/*par*S) and partition and post-segregational killing (*P*ω) (2,13,14). The ω_2 protein target site consists of two (*P*ω) or three (*Pcop*S) copies of a block composed of two direct and one inverted 7-bp repeats ($5'$-$^{A}/_{T}$ATCAC$^{A}/_{T}$-$3'$) symbolized by ⟶⟶⟵, plus one additional 7-bp direct repeat ⟶ downstream of the last block in *P*cop, or in the inverted ⟵ orientation downstream of the last block in *P*ω (see Fig. 1). Upstream of *P*δ, which overlaps with the *par*S site, there are seven head-to-tail direct 7-bp repeats and two inverted 7-bp repeats (Fig. 1). Such organization of binding sites has been well documented for eukaryotic transcription factors that bind cooperatively to tandemly repeated units [e.g., TFIIIA (15), STAT family of proteins (16), HSF protein (17), IRF family of proteins (18), MR-GR proteins (19), NR superfamily of proteins (TRE, VDR, RAR, RXR) (20–22)]. Here the relative

*To whom correspondence should be addressed. Tel: +34 585 4546; Fax: +34 585 4506; Email: jcalonso@cnb.uam.es

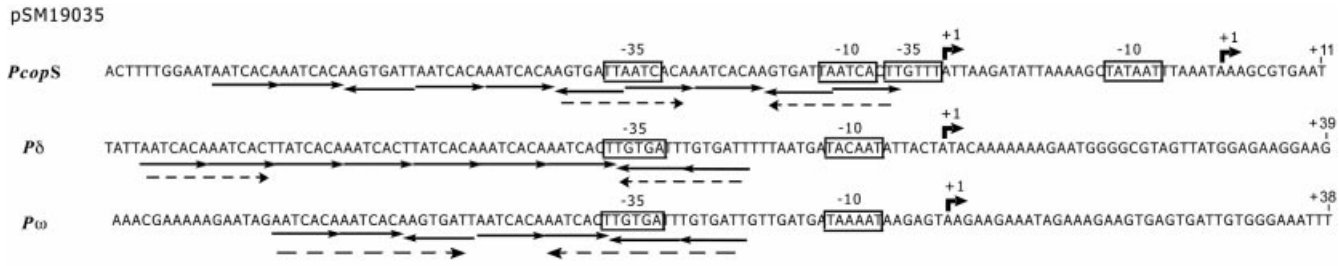

Figure 1. Comparison of the nucleotide sequences of the ω_2 targets. The conserved –35 and –10 regions of the *P*cops, *P*δ and *P*ω promoters are indicated as full line boxes. Bent arrows and +1 denotes known transcription start sites. The ω_2 protein binding 7 bp repeats and their relative orientations are indicated by arrows below the nucleotide sequences. Putative palindromic sequences are indicated by dashed convergent arrows below the nucleotide sequences.

orientation and spacing of the core recognition motifs play an essential role in the specificity of DNA-binding and transcriptional activation.

Using site-directed mutagenesis, electrophoretic mobility shift assay (EMSA), DNase I and hydroxyl radical footprinting, surface plasmon resonance (SPR), and spectroscopic studies we have examined the binding of ω_2 to various arrays of the 7-bp repeat. These experiments show that ω_2 binds with very low affinity and no specificity to a single 7-bp repeat. The binding of ω_2 to DNA, albeit with varying individual affinity, is achieved by units composed of two differently oriented repeats [($\longrightarrow_2$), ($\longrightarrow\longleftarrow$) and ($\longleftarrow\longrightarrow$)]. The inverted repeats ($\longrightarrow\longleftarrow$) and ($\longleftarrow\longrightarrow$) are palindromic as the sequences are related by a 2-fold rotation axis, whereas the directed repeats ($\longrightarrow_2$) are not. Clusters of three, four or more (as well as the full-length cognate recognition sites composed of up to 10 heptads) provide the highest stability to the ω_2–DNA complexes with dissociation constants in the 5 nM range (2). Circular dichroism (CD) studies indicate that ω_2 induces local conformational changes in DNA.

MATERIALS AND METHODS

Bacterial strains, plasmids and oligonucleotides

Escherichia coli BL21(DE3) and XL1-Blue strains, the *Bacillus subtilis* Pδ:*lac*Z, *rec*A4 strain and plasmids pUC18, pHP13-ω and pT712ω were previously described (2,23,24). pHP14-borne ω (pHP14-ω) and ωΔ19 gene (pHP14-ωΔ19) were used for β-galactosidase measurements. Oligonucleotides containing the specified number of heptads were synthesized with three flanking adenines (aaa) at the 5′-end and three guanosines (ggg) at the 3′-end [denoted in lower case letters, e.g., 5′-aaaAATCACAggg-3′ (symbolized $\longrightarrow$) or 5′-aaaTGTGATTggg-3′ ($\longleftarrow$)]. These oligonucleotides and their complementary strands were annealed, gel purified and joined to HindII-cleaved pUC18 DNA. The ligated material was transformed into XL1-Blue competent cells. The modified plasmids contain two heptads [pCB252 (5′-aaaAATCACAAATCACAggg-3′, $\longrightarrow_2$), pBC520 (5′-aaaTGTGATTAATCACAggg-3′,$\longleftarrow\longrightarrow$) and pCB474 (5′-aaaAATCACATGTGATTggg-3′, $\longrightarrow\longleftarrow$)], three heptads [pCB343 (5′-aaaAATCACAAATCACAAATC-ACAggg-3′, $\longrightarrow_3$), pCB251 (5′-aaaAATCACAAATC-ACATGTGATTggg-3′, $\longrightarrow_2\longleftarrow$)], and four heptads [pCB345 (5′-aaaAATCACAAATCACAAATCACAAAT-CACAggg-3′, $\longrightarrow_4$), pCB344 (5′-aaaAATCACAAATCAC-ATGTGATTTGTGATTggg-3′, $\longrightarrow_2\longleftarrow_2$) and pCB429 (5′-aaaAATCACAAATCACATGTGATTAATCACAggg-3′, $\longrightarrow_2\longleftarrow\longrightarrow$)]. In the HindIII–KpnI DNA fragments the heptads with flanking three adenosines at the 5′-end and three guanosines at the 3′-end are surrounded by the multi-cloning site of the vector (pUC18) composed upstream of 20 bp (5′-AGCTTGCATGCCTGCAGGTC-3′) and downstream of 19 bp (5′-GACTCTAGAGGATCCCCGG-3′). The resulting HindIII–KpnI DNA fragments are therefore 52 (one heptad), 59 (two heptads), 66 (three heptads) and 73 bp (four heptads) in length. The DNA fragments were purified and the expected sequences confirmed by sequencing.

Plasmids pCB426, pCB533, pCB427, pCB428 and pCB481 were constructed containing two directly repeated heptads separated by 1-bp (e.g., 5′-aaaAATCACA[A]A-ATCACAggg-3′, $\longrightarrow$[A]$\longrightarrow$), 2-bp ($\longrightarrow$[AT]$\longrightarrow$), 3-bp ($\longrightarrow$[ATA]$\longrightarrow$), 4-bp ($\longrightarrow$[ATAG]$\longrightarrow$), 5-bp ($\longrightarrow$[ATAGG]$\longrightarrow$), 6-bp ($\longrightarrow$[ATAGGG]$\longrightarrow$) and 7-bp ($\longrightarrow$[ATAGGGA]$\longrightarrow$). The constructs are surrounded by the multi-cloning site of the vector. The lengths of the HindIII–KpnI DNA fragments with insertions between heptads used for DNase I footprinting experiments are: 60 ($\longrightarrow$[1]$\longrightarrow$), 61 ($\longrightarrow$[2]$\longrightarrow$), 62 ($\longrightarrow$[3]$\longrightarrow$), 63 ($\longrightarrow$[4]$\longrightarrow$) and 66-bp ($\longrightarrow$[7]$\longrightarrow$).

Oligonucleotides containing two directly repeated heptads (5′-aaaAATCACAAATCACAggg-3′) were modified on one of the heptads by single base pair substitutions. The wild type (wt) nucleotide sequence of both strands was modified by replacing, at each position, one nucleotide by the other three nucleotides. The mutated oligonucleotides were annealed, gel purified, joined to HindII-cleaved pUC18 DNA and transformed into XL1-Blue competent cells. The DNAs of the clones were purified and the results of site-directed mutagenesis were confirmed by sequence analysis. Since nucleotides in the first and seventh position show natural $^{A}/_{T}$ variance they were consequently only mutated to C and G. In the following list of constructs the mutations are given in parentheses: pCB536 (A1→C), pCB537 (A1→G); pCB438 (A2→T), pCB439 (A2→G), pCB440 (A2→C); pCB501 (T3→A), pCB515 (T3→G), pCB502 (T3→C); pC521 (C4→T), pCB518 (C4→A), pCB482 (C4→G); pCB480 (A5→T), pCB522 (A5→C), pCB479 (A5→G); pCB444 (C6→T),

pCB443 (C6→A), pCB442 (C6→G); pCB446 (A7→C), pCB445 (A7→G).

Chemicals, DNA, enzymes, proteins and reagents

All chemicals were p.a. grade and purchased from Merck, Darmstadt, Germany. DNA restriction and modification enzymes, dNTPs, and poly[d(I-C)] were from Boehringer Mannheim, Germany. Ultrapure acrylamide was from Serva, Heidelberg, Germany. The broad protein molecular weight marker was obtained from Gibco-BRL, Barcelona, Spain.

The buffers used were: buffer A, 50 mM Tris–HCl pH 7.5, 10 mM $MgCl_2$, 50 mM NaCl, 2 mM DTE, 0.2 mM phenylmethylsulfonylfluoride, 5% glycerol; buffer B, 50 mM Tris–HCl pH 7.5, 10 mM $MgCl_2$, 50 mM NaCl.

For EMSA and footprinting experiments, the HindIII–KpnI DNA segments (59 bp, two heptads, 66 bp, three heptads and 73 bp, four heptads) or EcoRI–SphI DNA fragments (71 bp, three heptads; and 78 bp, four heptads), were end-labeled by the filling-in reaction using the Klenow enzyme at the HindIII or EcoRI sites, and gel purified.

For Biacore experiments single biotinylated (Bio) double stranded (ds) oligonucleotides containing the specified number of heptads, flanked by Bio-gtgcaat at the 5′-end and tattca at the 3′-end [one (20 bp, e.g., 5′-Bio-gtgcaatAATCACAtattca-3′, (⟶), two (27 bp) in ($⟶_2$) or (⟶ ⟵) orientation, three (34 bp) in the ($⟶_3$) or ($⟶_2⟵$) and four heptads 41 bp ($⟶_4$)] and their non-biotinylated complementary strands were annealed, purified and bound to the SPR chip.

Oligonucleotides for CD studies containing the specified number of heptads, flanked by gcg at the 5′-end and gg the 3′-end [one (12 bp, e.g., 5′-gcgAATCACAgg-3′), two (19 bp) ($⟶_2$), (⟶⟵) or (⟵ ⟶), three (26 bp) ($⟶_3$), and four heptads (33 bp) ($⟶_4$)] in the indicated orientation and their complementary strands were annealed and purified by ion exchange chromatography using a Mono Q column. The concentration of DNA is expressed as moles of nucleotides and was determined using a molar extinction coefficient of 6500 $M^{-1}cm^{-1}$ at 260 nm.

The ω_2 protein was purified as previously described (25,26). The protein concentration is expressed in moles of ω_2 dimers and was determined from the absorbance at 276 nm using an absorption coefficient of $A_{1\%,1cm} = 3.63$ (26).

Measurement of protein–DNA interactions

For EMSA, gel purified [^{32}P]HindIII–KpnI DNA (2 nM) was incubated with various amounts of ω_2 and in the presence of 1 μg poly [d(I-C)] as non-specific competitor DNA in buffer B for 15 min at 37°C in 20 μl final volume as previously described (2). The mixture was then separated using an 8% non-denaturing polyacrylamide gel electrophoresis (ndPAGE). The ndPAGE were run with 0.5× Tris–borate-EDTA (24) at 45 V at 4°C and dried prior to autoradiography.

To obtain apparent dissociation constant ($K_{d,app}$) values from EMSA and DNase I footprint experiments, concentrations of free DNA and ω_2–DNA complexes were densitometrically determined under non-saturating conditions from differently exposed autoradiographs of EMSA and DNase I footprinting gels. ω_2 protein concentrations that transfer 50% of the ^{32}P-DNA into complexes or protect 50% from DNase I digestion are approximately equal to the $K_{d,app}$ under conditions where the DNA concentration is much lower than $K_{d,app}$. Since DNA concentrations used in the EMSA and DNase I protection experiments are 2 nM, reliable results are expected for $K_{d,app}$ values above 20 nM. In SPR experiments, the ω_2 protein concentrations at 50% of the maximal resonance units (RU) values were taken as equivalent to $K_{d,app}$. The reaction conditions for DNase I footprint experiments were as for EMSA. DNase I treatment was as previously described (2). The samples were resuspended in loading buffer [80% (v/v) formamide, 1 mM EDTA, 0.1 % (v/v) bromophenol blue and 0.1% (v/v) xylene cyanol], separated in 15% denaturing PAGE (dPAGE) and were autoradiographed. For size control marker, ladders obtained with the chemical sequencing reaction (G+A) on the same DNA fragments were used.

SPR was measured in real time as previously described (27) using a Biacore 2000 instrument with biotinylated synthetic DNA immobilized on a Streptavidin sensor chip. By construction, all chips contained the same molar concentration of heptads, although the number of heptads per DNA molecule was different. After the DNA segments were coupled to the streptavidin-coated surface of the flow cells, kinetics of binding were measured with ω_2 concentrations ranging from 0.8 to 100 nM. The SPR signal was measured in RU, 100 RU corresponding to 0.1 ng/mm^2 of ω_2 bound to the chip. The rate and equilibrium binding constants and Hill coefficients were calculated using BIAevaluation 3.0 software.

Hydroxyl radical footprinting was performed as previously described (28). [α^{32}P]HindIII–KpnI or EcoRI–SphI DNA (2 nM) and 1 μg of poly [d(I-C)] as non-specific competitor DNA were incubated with various amounts of ω_2 protein in a total volume of 20 μl in buffer B. After 20 min incubation at 30°C, the footprint was started by addition of 3 μl of a freshly prepared solution containing 4 mM EDTA, 2 mM ammonium iron(II)-sulfate hexahydrate, 14 mM sodium ascorbate and 1.5% H_2O_2. After 4 min, the reaction was stopped by addition of 2 μl of 100 mM thiourea and 2 μl of 0.5 M EDTA. Samples were diluted 1:1 with water, and the DNA ethanol precipitated. The samples were resuspended in loading buffer separated in 15% dPAGE, and the gels were autoradiographed. For the analysis of the footprint the intensities of random bands (6 to 8), in each lane, outside the footprinting area were added and used to obtain a normalization factor. This factor served to correct any potential loading error in the different lanes. The normalized band intensities of protein-free control were then subtracted from the corresponding band intensities of the lanes of the protein-containing DNA.

CD spectra in the 320–250 nm region were measured at 20°C using a Jasco J720 spectropolarimeter. For titration of DNA with ω_2 protein, aliquots of a concentrated ω_2 solution in buffer B were added to the desired DNA solutions in a 5 mm path-length cuvette, mixed and incubated for 15 min at 20°C before measurements. For the calculation of the stoichiometries the ellipticity differences at 264 nm between ω_2:DNA complexes and free DNA was plotted versus the molar ratio ω_2:DNA.

RESULTS

ω_2 protein binds to heptad repeats with different orientation

In pSM19035, upstream of the *cop*S, δ and ω genes there are 10, nine and seven copies of the 7 bp repeat 5′-$^{A}/_{T}$ATCAC$^{A}/_{T}$-3′, respectively (Fig. 1). These heptads are the suspected ω_2 binding sites (2); however, alternative ω_2 protein binding sites have not been formally ruled out (see dashed arrows in Fig. 1).

Using EMSA we studied the complex formation of ω_2 with the 59 to 73 bp long [α-^{32}P]HindIII–KpnI DNA fragments containing one to four unspaced heptads as a function of ω_2 protein concentration. We failed to detect binding of ω_2 (up to 500 nM) to DNA fragments containing only one heptad. The $K_{d,app}$ that were obtained from EMSA are summarized in Table 1.

The ω_2 protein concentration required to bind 50% of the DNA containing two heptads in the head-to-head ⟶⟵ configuration is apparently lower than for binding DNA containing heptads in the $\longrightarrow_2$ or ⟵ ⟶ orientation. The $K_{d,app}$ values (equivalent to the ω_2 concentration required to protect 50% of the DNA) are 20, 90 and 120 nM, respectively (Fig. 2B, A and C, Table 1). Only one shifted band was observed with heptads in the $\longrightarrow_2$, ⟶⟵ and ⟵ ⟶ orientation (Fig. 2A to C denoted by arrowheads).

The affinity of ω_2 binding to DNA containing three and four heptads (Fig. 2D–H) is similar to full-length sites (4–12 nM) (2). With the exception of diheptads (Fig. 2A–C) and of DNA in the $\longrightarrow_2\longleftarrow$ ⟶ configuration where only one shifted band was observed (Fig. 2H), the formation of higher order complexes was observed for DNA with increased number of adjacent heptads. One to three shifted bands were observed when the DNA fragment encompassed three or four heptads, respectively (denoted by brackets in Fig. 2D–G). This indicates that the 7-bp heptads are the binding site for ω_2 protein and that a minimum of two heptads is required for initial binding. This rules out the binding of ω_2 protein to alternative sites, as the palindromic sequences denoted by dashed converging arrows in Figure 1. The observed heterogeneity of formed complexes suggests a varying occupancy of the heptad binding sites by ω_2 and/or a distortion of the DNA segments.

ω_2 protein protects large DNA segments against DNase I attack

To study the effect of ω_2 on the protection of DNA fragments containing two to four heptads in different orientations, the ω_2–DNA complexes were analyzed by DNase I footprinting. Protein ω_2 failed to protect a DNA fragment containing only one heptad from DNase I attack (data not shown) whereas discrete regions of DNA containing two to four heptads were protected. In most of the studied DNA fragments the protected region is longer than the stretch of heptad sequences, namely ~18 bp in length for $\longrightarrow_2$ (Fig. 3A), ~22 bp for ⟶⟵ (Fig. 3B), ~28 bp for $\longrightarrow_2\longleftarrow$ (Fig. 3D) and $\longrightarrow_3$ (Fig. 3E) and ~36 bp for $\longrightarrow_4$ (Fig. 3F) and $\longrightarrow_2\longleftarrow_2$ (Fig. 3G). The protection is mainly extended at the upstream ends of the dsDNA. As shown in Figure 3C and H, the protected regions from DNase I attack were shorter than the heptad stretches with ω_2 protein protecting only ~12 bp in a DNA segment containing two heptads in the ⟵ ⟶ orientation and ~26 bp in a DNA fragment with four heptads in $\longrightarrow_2\longleftarrow\longrightarrow$ orientation. In the latter case, the upstream region and the first three heptads were protected from DNase I attack by ω_2, but the fourth heptad (at the 3′-end) was not protected (Fig. 3H).

With the exception of heptads in the ⟵ ⟶, $\longrightarrow_2\longleftarrow_2$ and $\longrightarrow_2\longleftarrow$ ⟶ orientations (Fig. 3C, G and H) where single sensitive sites interrupted by protected regions were observed, continuous protection from DNase I attack by ω_2 were found with DNA containing two (⟶⟵ and $\longrightarrow_2$), three ($\longrightarrow_2\longleftarrow$ and $\longrightarrow_3$) and four ($\longrightarrow_4$) heptads (Fig. 3A, B, D, E and F). Protection from DNase I attack was also observed in the upstream region, where heptads were not present, with DNA containing two (⟶⟵ and $\longrightarrow_2$), three ($\longrightarrow_2\longleftarrow$ and $\longrightarrow_3$) and four ($\longrightarrow_4$) heptads (Fig. 3A, B, D–F). As previously postulated (2), this is most likely caused by formation of a large nucleoprotein complex in which non-specific binding of ω_2 to the flanking DNA regions is nucleated from the *Pcop*S, *P*ω and *P*δ or *par*S region (see Fig. 1).

The protection effect of ω_2 was quantified by densitometric scanning of the autoradiographs (see Fig. 3). Protein ω_2 binds with similar affinity to two heptads with the ⟶⟵ or $\longrightarrow_2$ orientation ($K_{d,app}$ ~25 nM) and three and four heptads ($K_{d,app}$ 5–12 nM) (Table 1).

There is a difference in the $K_{d,app}$ as determined by EMSA and DNase I for ω_2–DNA complexes with the heptads in the $\longrightarrow_2$ orientation ($K_{d,app}$ 90 and 25 nM, respectively) when compared to the ⟶⟵ orientation ($K_{d,app}$ ~25 nM in both cases), which might suggest a faster off rate of ω_2 for $\longrightarrow_2$ DNA under the conditions of EMSA. The ω_2 concentrations required to protect 50% of the tail-to-tail (⟵ ⟶) DNA segments are similar when determined with both EMSA and DNase I footprinting ($K_{d,app}$ ~130 nM) (Table 1).

Table 1. $K_{d,app}$ in nM of ω_2 necessary to achieve half saturation of 2 nM DNA

Orientation and number of heptads	EMSA	DNase I footprinting	SPR
$\longrightarrow$	>500	>500	>500
$\longrightarrow_2$	~90	~25	~20
⟶⟵	~20	~25	~20
⟵ ⟶	~120	~140	ND
$\longrightarrow_3$	~12	~12	~10
$\longrightarrow_2\longleftarrow$	~12	~12	~10
$\longrightarrow_4$	~8	~7	~6
$\longrightarrow_2\longleftarrow_2$	~6	~8	ND
$\longrightarrow_2\longleftarrow$ ⟶	~14	~14	ND
$(\longrightarrow_2\longleftarrow)_3\longrightarrow$	~4	~5	~6

ND, not determined.

Kinetics of ω_2 protein binding to DNA

SPR experiments provided $K_{d,app}$ values similar to those determined by DNase I footprinting assays for ω_2–DNA complexes containing different numbers and orientations of heptads (Table 1). The affinity of ω_2 to DNA containing a single heptad is low with $K_{d,app} > 1$ μM (Fig. 4A, Table 1). Protein ω_2 binds to DNA containing two 7-bp repeats in the $\longrightarrow_2$ or ⟶⟵ orientation with similar affinity ($K_{d,app}$ ~20 nM), hence only the former was shown (Fig. 4B).

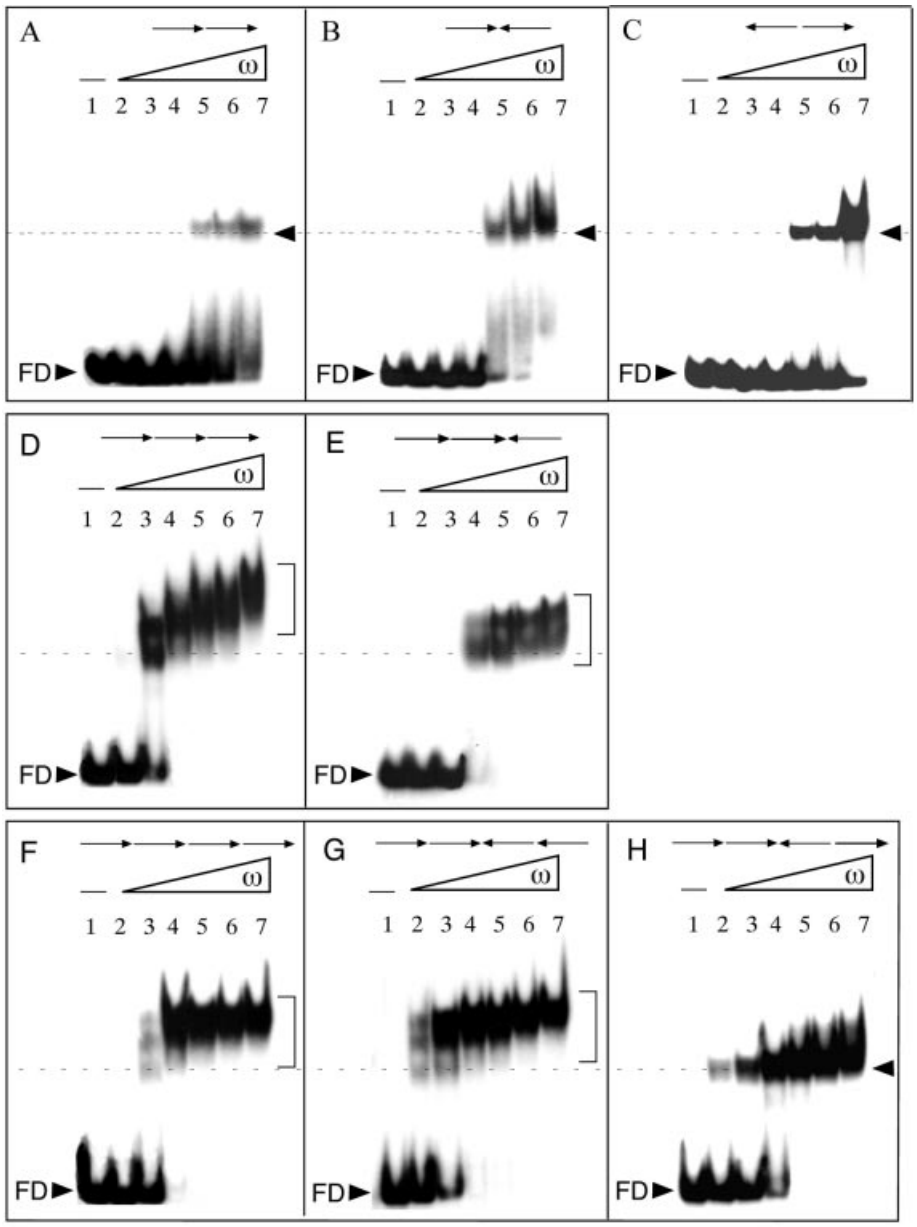

Figure 2. Interaction of ω_2 protein with DNA containing two to four heptads in different orientations. The 59 [(**A**–**C**) two heptads], 66 [(**D** and **E**) three heptads] and 73 bp [(**F**–**H**) four heptads] [α-^{32}P]HindIII–KpnI DNA (2 nM) and 1 µg of poly[d(I-C)], as non-specific competitor DNA, were incubated with increasing concentrations of ω_2 in buffer B for 15 min at 37°C. The formed ω_2–DNA complexes were analyzed by EMSA. The arrows at the top of the gels indicate number and orientation of the 7 bp repeats. An arrowhead or a bracket to the right of the bands indicates the type(s) of ω_2–DNA complexes. A broken line indicates the position of the fastest moving complexes, detected at low protein concentration. Except in (C), the ω_2 protein concentrations were 4, 8, 16, 32, 64 and 128 nM (lanes 2–7, respectively). In (C) the ω_2 concentrations were 8, 16, 32, 64, 128 and 256 nM. The symbol – in lane 1 indicates the absence of protein, FD labels the band due to free DNA.

The association ($k_a \sim 1 \times 10^7$ ms^{-1}) and dissociation (k_d ~0.1 s^{-1}) rate constants are similar for ω_2 binding to DNA containing three heptads in $\longrightarrow_2\longleftarrow$ (Fig. 4C) and $\longrightarrow_3$ orientation and to DNA containing four heptads in the $\longrightarrow_4$ orientation (Fig. 4D). Although the different chips are coated with the same number of binding sites, the moles of bound DNA differ according to the different number of heptads per DNA molecule. We assume that differences in conformation of the DNA targets account for the small differences in $K_{d,app}$ between targets with two (20 nM) and three or four repeats ($K_{d,app}$ 6–10 nM) and not the statistical degeneracy of the macroscopic binding constant (29). A similar binding affinity was observed when the full-length site (Fig. 1) containing seven to 10 repeats ($K_{d,app}$ 4–10 nM) was studied (2).

Binding of ω_2 protein induces conformational changes in DNA

Titration of DNA containing two $\longrightarrow_2$, three $\longrightarrow_3$ and four $\longrightarrow_4$ direct heptads (Fig. 5A–C) with ω_2 was accompanied by spectral changes in the DNA region between 250 and 320 nm.

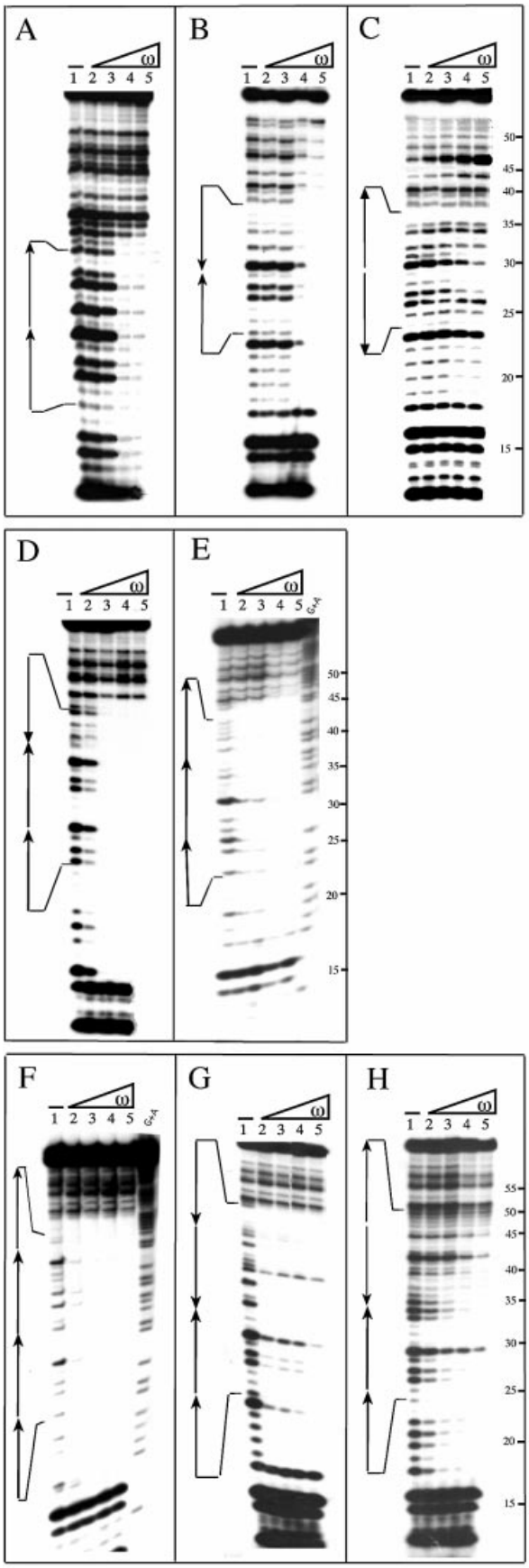

Isosbestic points were found at 283 nm for DNA with two heptads, $\longrightarrow_2$, and at 282 nm for DNA with three $\longrightarrow_3$ and at 281 nm for DNA with four heptads, $\longrightarrow_4$. The positions of the isosbestic points indicate that the CD spectra are mainly determined by two components, namely free DNA and complexes with ω_2. The CD spectra do not discriminate between complexes differing in the number of ω_2 and position of ω_2 occupying the two, three and four binding sites per DNA. At substoichiometric amounts of ω_2 the CD spectra do not allow to deduce the possible formation of complexes with varying stoichiometry as suggested by the EMSA experiments shown in Figure 2.

Plots of $\Delta[\Theta]_{264nm}$, the difference in the ellipticity at 264 nm between ω_2-DNA and free DNA, versus molar ratio of ω_2 to DNA containing two $\longrightarrow_2$ (Fig. 5D), three $\longrightarrow_3$ (Fig. 5E) or four $\longrightarrow_4$ heptads (Fig. 5F) showed stoichiometries of binding of 2.2, 3.1 and 4.5 ω_2 per DNA with two, three and four heptads, respectively. These results, which are close to the binding of one ω_2 to one DNA heptad, indicate that each dimer binds to each half of the minimal binding site and interacts with the neighboring dimer.

Sequence selective recognition by ω_2 protein

To learn about the relevant nucleotides involved in ω_2 binding, we have substituted every base pair of the upstream heptad (5′-$^{A}/_{T}$ATCAC$^{A}/_{T}$-3′, positions 1 to 7) of the $\longrightarrow_2$ binding site, whereas the downstream heptad (positions 1′ to 7′) was not modified (Table 2). The protein concentration required to protect 50% of the 59-bp HindIII–KpnI target DNA from DNase I attack was determined. The replacement of A at position 1 or 7 by T (A→T, a natural one), A→C or A→G does not affect the ω_2 footprinting ($K_{d,app}$ ~ 20 nM), and the presence of a C at positions 1 or 7 slightly increases (2-fold) ω_2 protection to DNase I attack (see above). The A→T or A→G replacements at position 2 do not seem to affect the ω_2 binding, but A→C reduced by 8-fold ω_2 protection from DNase I attack (Table 2). The T→G replacement at position 3, C→A or C→G at position 4 and A→G or A→T replacements at position 5 or replacement of C at position 6 for any other base pair reduced ω_2 protection from DNase I attack by >7-fold (Table 2). The other replacements revealed an intermediate affinity for ω_2 (Table 2).

The base specific effects of changes in positions 2 and 3 and more general effects of base pair exchanges in positions 4 to 6, which drastically affect the binding of ω_2 to a diheptad DNA, suggest that: (i) the ω_2 operator site consists of two highly similar heptads, (ii) each heptad defines an *operator half site*

Figure 3. DNase I footprinting experiments of ω_2–DNA complexes. The [α-^{32}P]HindIII–KpnI DNA fragments (bottom strand) described in Figure 2 (containing two to four heptads) were used. The number, location and orientation of the 7 bp repeats are indicated by arrows. [α-^{32}P]DNA (2 nM) and 1 μg of poly [d(I-C)], as non-specific competitor DNA, were incubated with increasing concentrations of ω_2 in buffer B for 15 min at 37°C, followed by limited digestion with DNase I. Except in (**C**), the ω_2 concentrations were 8, 16, 32 and 64 nM (lanes 2–5, respectively). In (C) the ω_2 concentrations were 32, 64, 128 and 256 nM. The symbol – in lane 1 indicates the absence of ω_2. The G+A lanes at the right of (**E**) and (**F**) were obtained by chemical sequencing reaction (Maxam–Gilbert) and used as size standard. The numbers to the right of (C), (E) and (**H**) refer to nucleotide positions in the sequence of the studied DNA.

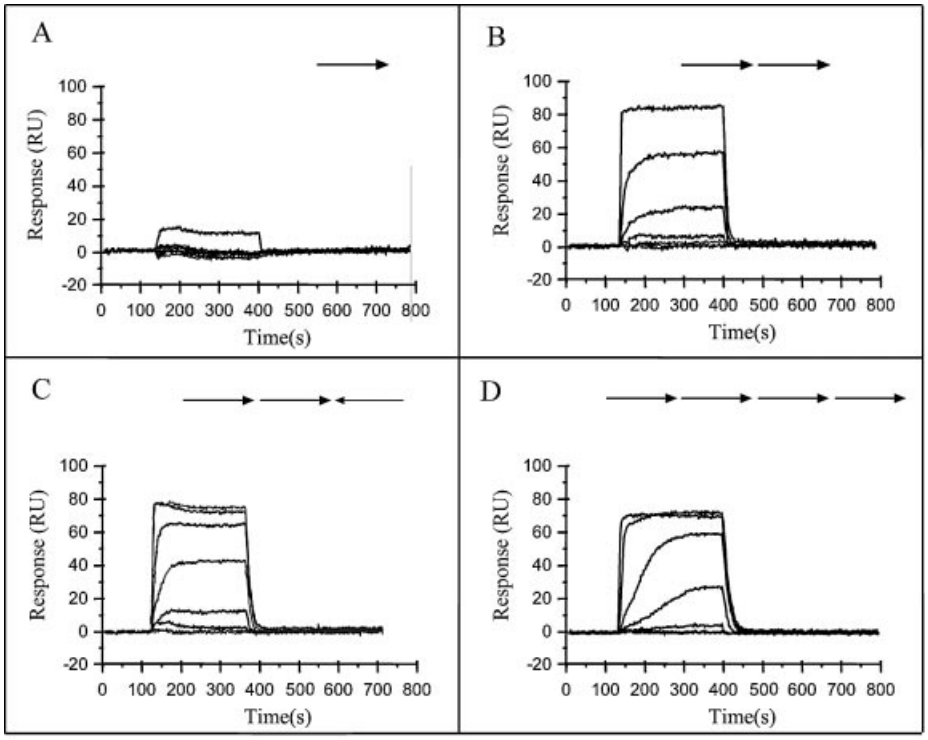

Figure 4. SPR studies of the interaction of ω_7 protein with its target sites. DNA segments containing one (**A**), two (**B**), three (**C**) and four (**D**) heptads with total lengths of 20, 27, 34 and 41 bp, respectively, have been used. The nucleotide sequences are presented in Materials and Methods and number and orientation of the heptads are indicated by arrows. The sensograms were obtained at different ω_2 concentrations (1.6, 3.2, 6.4, 12.5, 25, 50, 100 and 200 nM). Several curves overlap at low ω_7 concentrations [three and two curves in (C) and (D), four curves in (B), and seven curves in (A)].

and (iii) the pentameric central 5′-ATCAC-3′or its complementary sequence is relevant for ω_2 binding. Identical results were obtained when the mutations were introduced in one of the repeats of two inversely oriented heptads (data not shown).

ω_2 protein interacts with the 5′-ATCAC-3′ central core

Hydroxyl radical footprinting of ω_2–DNA complexes with DNA containing two ($\longrightarrow_2$) and four ($\longrightarrow_4$) heptads showed a different protection pattern at both DNA strands. The distribution of protected positions at the 'top' strand was different to that observed at the 'bottom' strand, suggesting that ω_2 interacts differently with each strand. As revealed in Figure 6A and B, the bases at the 'top' strand that were protected by ω_2 protein on a $\longrightarrow_4$ DNA segment from the attack of hydroxyl radicals cluster in the 5′-AT-3′ or 5′-ATC-3′ sequence (positions 2 and 3 or 2 to 4). The protected bases of the first heptad cannot be quantified due poor resolution of the gel. The protected regions on the other three heptads are separated by four or five non-protected nucleotides (Fig. 6B). On the 'bottom' strand the bases protected by ω_2 protein cluster in the 5′-GTG-3′ sequence (positions 4 to 6). Here the protected bases of the fourth heptad cannot be quantified due poor resolution of the gel. The protected regions on the three heptads are separated by four non-protected nucleotides (Fig. 6C).

Hydroxyl radical footprinting of a ω_2–DNA complex with DNA containing three heptads in the $\longrightarrow_2\longleftarrow$ orientation was also assayed (Fig. 7A–C). On the 'top' strand the bases protected on the two directly repeated heptads cluster in the 5′-AT-3′ or 5′-ATC-3′ sequence and in the inversely repeated heptad they cluster in the 5′-GTG-3′ sequence (Fig. 7C). On the 'bottom' strand the protected bases cluster in the 5′-GTG-3′ sequence of the directly repeated heptads and in the 5′-AT-3′ or 5′-ATC-3′ sequence of the inversely repeated heptad (Fig. 7A and B).

ω_2 protein binds poorly to a spaced core binding motif

The ω_2 protein probably binds to the DNA major groove with two anti-parallel β-strands, featuring two arginines (Arg31, Arg31′) that point to the base pairs and possibly recognize both guanines (10). In a previous section it is shown that: (i) a mutation at the central core of the upstream heptad in $\longrightarrow_2$ configuration for any other nucleotide reduces ω_2 binding >8-fold compared to the cognate site (Table 2), and (ii) ω_2 protein specifically protects the 5′-ATCAC-3′ segment of the heptads.

To address whether the protein binds to a spaced target site, the spacing of two direct ω_2 core motifs was varied by 1 ($\longrightarrow$[1]$\longrightarrow$) to 7 bp ($\longrightarrow$[7]$\longrightarrow$), and the protection of DNA by bound ω_2 protein was determined by DNase I footprinting. All these separated heptads failed to form measurable ω_2–DNA complexes in the presence of up to 40 nM ω_2. Half maximal saturation was observed in the presence of 100–120 nM ω_2 to diheptads separated either by 1 ($\longrightarrow$[1]$\longrightarrow$) to 7 bp ($\longrightarrow$[7]$\longrightarrow$) indicating a 5- to 6-fold reduced binding affinity when compared with the unspaced cognate $\longrightarrow_2$ site ($K_{d,app}$ ~20 nM). Identical results were obtained when the spacing of two inversely oriented heptads

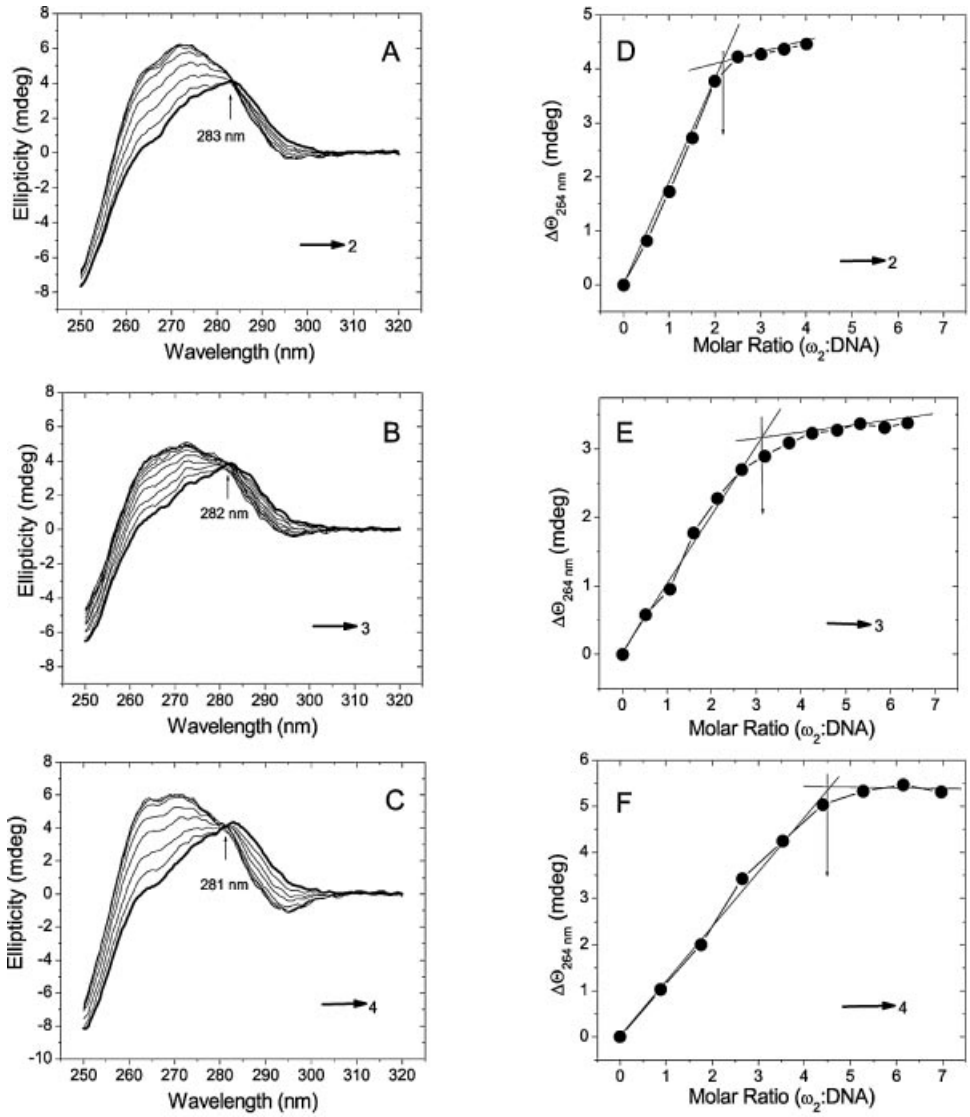

Figure 5. Titration of DNA with ω_2 protein. CD spectra of DNA with two heptads in the $\longrightarrow_2$ orientation (**A**), three heptads in the $\longrightarrow_3$ orientation (**B**) and four heptads in the $\longrightarrow_4$ orientation (**C**) are shown. Free DNA is indicated by thick lines, the DNA start concentrations are 3.2 (A), 2.09 (B) and 2.09 μM (C); ω_2 concentrations increase from 1.6 to 10.1 μM (A), 1.8 to 12.7 μM (B) and 1.8 to 12.8 μM (C). In (**D**), (**E**) and (**F**) is plotted the ellipticity increase at 264 nm induced in solutions of DNA [data from (A), (B) and (C), respectively] versus the ω_2:DNA molar ratio. Saturation is achieved at molar ratios of ~2.2:1, ~3.1:1 and ~4.5:1 with DNA containing two, three and four heptads, respectively. The samples were in buffer B at 20°C.

($\longrightarrow$[1] $\longleftarrow$ to $\longrightarrow$[7] $\longleftarrow$) were used (data not shown). Similarly the Arc repressor binds poorly to spaced half sites (30).

DISCUSSION

The DNA binding site of ω_2 at the *Pcop*S, *P*δ and *P*ω promoter regions is composed of an array of adjacent unspaced heptads (see Fig. 1). Unlike the Arc dimers, which bind to each subsite with nanomolar affinities (31), the ω_2 protein binds with low affinity ($K_{d,app}$ > 1 μM) to a subsite or single heptad. The ω_2 protein binds with high specificity and affinity to two ($K_{d,app}$ ~ 20 nM) or more unspaced heptads ($K_{d,app}$ 4–12 nM). The characterization of several heptads in different orientation has led to the identification of a consensus ω_2 operator site composed of two conserved and unspaced heptads (5′-$^{A}/_{T}$ATCAC$^{A}/_{T}$-3′) to which two ω_2 bind with high affinity. This is consistent with stoichiometry experiments that show that 2.2, 3.1 and 4.5 ω_2 molecules bind DNA segments containing two, three and four heptads, respectively. It is likely, therefore, that each heptad defines an operator half-site.

A reduced (3- to 6-fold) ω_2 binding affinity to two heptads spaced by 1 to 7 bp was observed. Similar results have been reported for other members of the RHH protein family when the binding site was artificially spaced (30,32). Each ω_2 protein contacts a 3 to 5 bp sequence in each DNA half site (heptad) (33; this work). Heptads in inverted $\longrightarrow\longleftarrow$ and divergent $\longleftarrow\longrightarrow$ orientations have palindromic symmetry, which allows the symmetry-related binding of two ω_2 proteins to each of the two heptads, whereas ω_2–DNA complexes with

Table 2. Binding of ω_2 protein to DNA studied by DNase I protection experiments

Modified position	Nucleotide position[a]	[ω_2] required to reach $K_{d,app}$ (in nM)
	1 2 3 4 5 6 7 1′ 2′ 3′ 4′ 5′ 6′ 7′	
–	5′-…a A T C A C a a A T C A C a …-3′	~20
1	5′-…C ⟶ ⟶...-3′	~10
1	5′-…G⟶ ⟶...-3′	~20
2	5′-... —T ⟶ ⟶…-3′	~20
2	5′-... —C ⟶ ⟶…-3′	>160
2	5′-... —G ⟶ ⟶…-3′	~20
3	5′-…——A⟶ ⟶…-3′	~80
3	5′-…——C⟶ ⟶…-3′	~80
3	5′-…——G⟶ ⟶…-3′	~160
4	5′-…———T ⟶ ⟶…-3′	~80
4	5′-…———A ⟶ ⟶…-3′	~160
4	5′-…———G ⟶ ⟶…-3′	>160
5	5′-… ————T ⟶ ⟶…-3′	>160
5	5′-… ————C ⟶ ⟶…-3′	~160
5	5′-… ————G ⟶ ⟶…-3′	~160
6	5′-… ————T⟶ ⟶…-3′	>160
6	5′-… ————A⟶ ⟶…-3′	>160
6	5′-… ————G⟶ ⟶…-3′	>160
7	5′-... ————C ⟶…-3′	~10
7	5′-… ————G ⟶…-3′	~20

The DNA contained two directly repeated heptads of which the upstream one was mutated by one base in consecutive positions as shown on each line.
[a]The heptad sequences are flanked by three adenines at the 5′-ends and three cytosines at the 3′-ends and surrounded by the multi-cloning site of the vector. The base pair difference with wt is highlighted.

adjacent heptads in tandem orientation $\longrightarrow_2$ are not symmetry-related. The interfaces between ω_2 in complexes with symmetry-related and non-symmetry-related heptads $\longrightarrow_2$ might be different. Except EMSA, DNase I and chemical footprinting and SPR techniques showed that ω_2 protein binds with comparable high affinity to diheptads in $\longrightarrow_2$ or $\longrightarrow\longleftarrow$ orientation, $K_{d,app}$ ~20 nM, but binds to a diheptad in the $\longleftarrow\longrightarrow$ orientation with ~6-fold lower affinity, $K_{d,app}$ ~130 nM.

Three heptads in $\longrightarrow_3$ or $\longrightarrow_2\longleftarrow$ orientation or four heptads in the $\longrightarrow_4$, $\longrightarrow_2\longleftarrow\longrightarrow$ or $\longrightarrow_2\longleftarrow_2$ orientations form high affinity binding sites for ω_2 protein, as judged by EMSA, DNase I footprinting or SPR. The affinity of these heptads is comparable to that observed with the full-length binding site (2). All these data are consistent with the observation that the affinity of ω_2 for a specific promoter does not increase by increasing the number of heptads in the respective operator, provided that there are at least three or four heptad repeats (2; this work). Upon binding to its cognate site, ω_2 protein at high concentration has the tendency to polymerize on the 5′ region of the 'top' strand (2), an effect that has yet to be understood.

Genetic and biochemical experiments show that the bases of the 5′-ATCAC-3′ core or the complementary 5′-GTGAT-3′ sequence are essential for the interaction of ω_2. Hydroxyl radical footprints show that ω_2 mainly interacts with the central 5′-TCA-3′ sequence. This has been confirmed by Raman spectroscopy, showing that the central 5′-TCA-3′ motif of the heptads might be the main target site for ω_2 binding to operator DNA (34).

The N-terminal regions (1–23 and 1–22 in subunits I and II, respectively) of ω_2 are not defined in the electron density due to proteolysis during crystallization and partial disorder (10). *In vivo* experiments demonstrated that plasmid-based ω_2 variants lacking the first 20 residues specifically repress utilization of a chromosomal-based *P*δ promoter (F. Pratto, unpublished results). It is likely therefore that the flexible N-terminus is not involved in binding of ω_2 protein to operator sequences. According to a preliminary model ω_2 protein binds to the DNA major groove with the two anti-parallel β-strands (formed by residues Lys28 to Val32 and Lys28′ to Val32′) (10).

The operator sites of other RHH proteins (namely the MetJ, Arc and CopG proteins) show an overall bend of ~50–60° in the protein–DNA complexes (7,9,33). This agrees with CD titration experiments that show conformational changes in DNA upon ω_2 binding, and Raman spectra indicate an induced fit of both, ω_2 and DNA, as shown by changes in vibrational modes of deoxyribose moieties and protein-induced DNA bending (34). By contrast, DNase I footprint experiments did not indicate the presence of hypersensitive sites upon ω_2 binding to its cognate site (see Fig. 3).

Crystal structures of repressor–DNA complexes of MetJ (6), Arc (7,8) and CopG (9) have shown that these repressors bind as two dimers to palindromic operator sites. MetJ binds symmetrically to tandem binding sites (6), whereas the interaction of Arc and CopG with their palindromic cognate sites is asymmetric (7,9). The distances between the binding centers of the two dimers on the DNA are different: MetJ 8 bp apart, Arc 11 bp apart, Mnt and CopG each 9 bp apart. The β-ribbon of each of the repressors comprises seven to nine amino acid residues per monomer in MetJ, Arc, Mnt and CopG. By contrast, only five amino acid residues form the β-ribbon in ω_2 protein (10) and the centers of the half-sites are only 7 bp apart in agreement with the heptad repeat structure of operator DNA. For any heptad orientation ($\longrightarrow\longleftarrow$, $\longrightarrow_2$ or $\longleftarrow\longrightarrow$) the 5′-TCA-3′ motifs are separated by a center-to-center spacing of 7 bp and rotated relative to each other by $7 \times 34° = 238°$. Therefore, like MetJ (32), ω_2 bound to seven to 10 heptads should wrap around the DNA helix.

Figure 8 shows a model of the ω_2–DNA complex that is based on the MetJ–DNA complex as the RHH motifs are

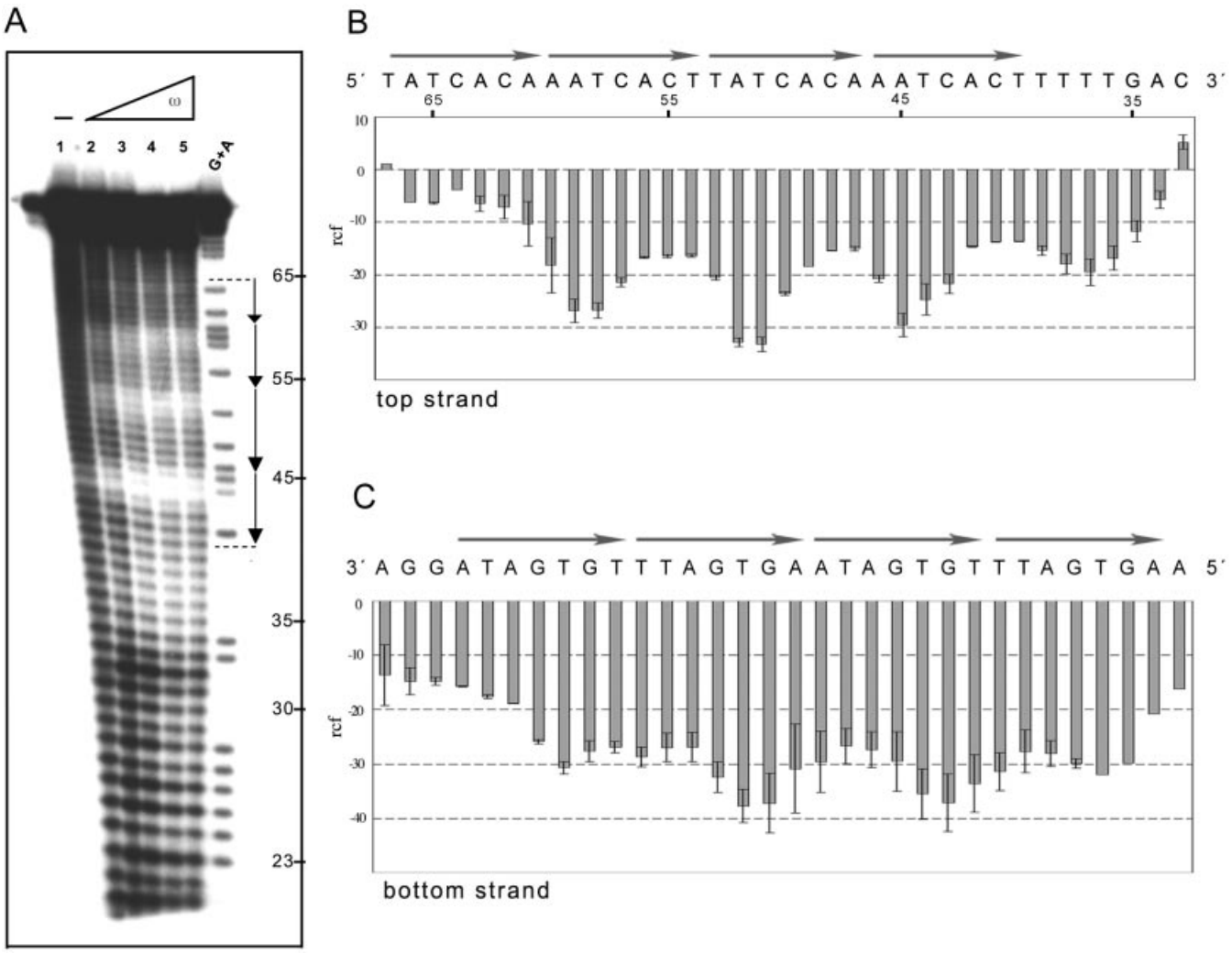

Figure 6. Hydroxyl radical footprinting of ω_2 protein bound to DNA with four heptads. The 78 bp [α-^{32}P]EcoRI–SphI [top strand (**A** and **B**)] or the 73 bp [α-^{32}P]HindIII–KpnI [bottom strand (**C**)] (2 nM) with four DNA heptads in $\longrightarrow_4$ orientation, in the presence of 1 µg of poly[d(I-C)] as non-specific competitor DNA, was incubated with increasing concentrations of ω_2 for 15 min at 37°C in buffer B, followed by hydroxyl radical footprinting. The ω_2 concentrations were 8, 16, 32 and 64 nM (lanes 2–5). The symbol – in lane 1 indicates the absence of protein. The G+A bands were used as size standards. The nucleotide sequence of the $\longrightarrow_4$ DNA and the histogram of the hydroxyl radical footprinting of the top (**B**) and bottom (**C**) strands, are shown. The relative cleavage frequency (arbitrary units) of the bound DNA compared to the unbound control is shown. Error bars show standard deviations and represent average values from three independent experiments.

comparable (6,10,32). It illustrates the gross arrangement of three ω_2 bound to a straight B-DNA segment composed of three heptads ($\longrightarrow_3$), each ω_2 inserting its antiparallel β-ribbon into the major groove of the DNA. The β-ribbon of ω_2 contains residues R31 on one β-strand and R31′ on the other strand that are related by a 2-fold rotation axis relating the two monomers in the dimer (10). The side-chains of R31 and R31′ are candidates for asymmetric contacts with guanines on the same DNA strand (motif 5′-CAC-3) in the $\longrightarrow_2$ diheptad or for symmetric contacts with guanines on the opposite strand in the $\longrightarrow\longleftarrow$ diheptad (10). Since protein ω_2 binds to seven to 10 heptads: ω_2 possibly decorates the DNA helix, adjacent ω_2 being rotated relative to each other by 252° around the DNA helix axis. The distance between ω_2 α-helices A can easily be reduced to become comparable to the distance in MetJ–DNA if DNA is bent (see above) or ω_2 slightly rotated on the heptad binding site. Figure 8 also shows that due to the 2-fold symmetry in the ω_2 dimer, two ω_2 bound to two heptads in head-to-tail orientation, $\longrightarrow_2$ is comparable to two ω_2 bound to $\longrightarrow\longleftarrow$ DNA. However, depending on the heptad orientation, different helices would interact. In the $\longrightarrow_2$ situation α-helices A' and A were located in close neighborhood at the surfaces of the two dimers, whereas in the $\longrightarrow\longleftarrow$ case α-helices A' of both ω_2 should be involved in interdimer interaction. In any case possible interactions between neighboring ω_2 bound to multiple heptads should sensitively depend on the spacing between the heptads, as actually observed (see above).

ACKNOWLEDGEMENTS

We thank Mrs B. Kannen for technical assistance during the spectroscopic measurements. This work was partially supported by grants BMC2003-00150 from MCT-DGI to J.C.A.,

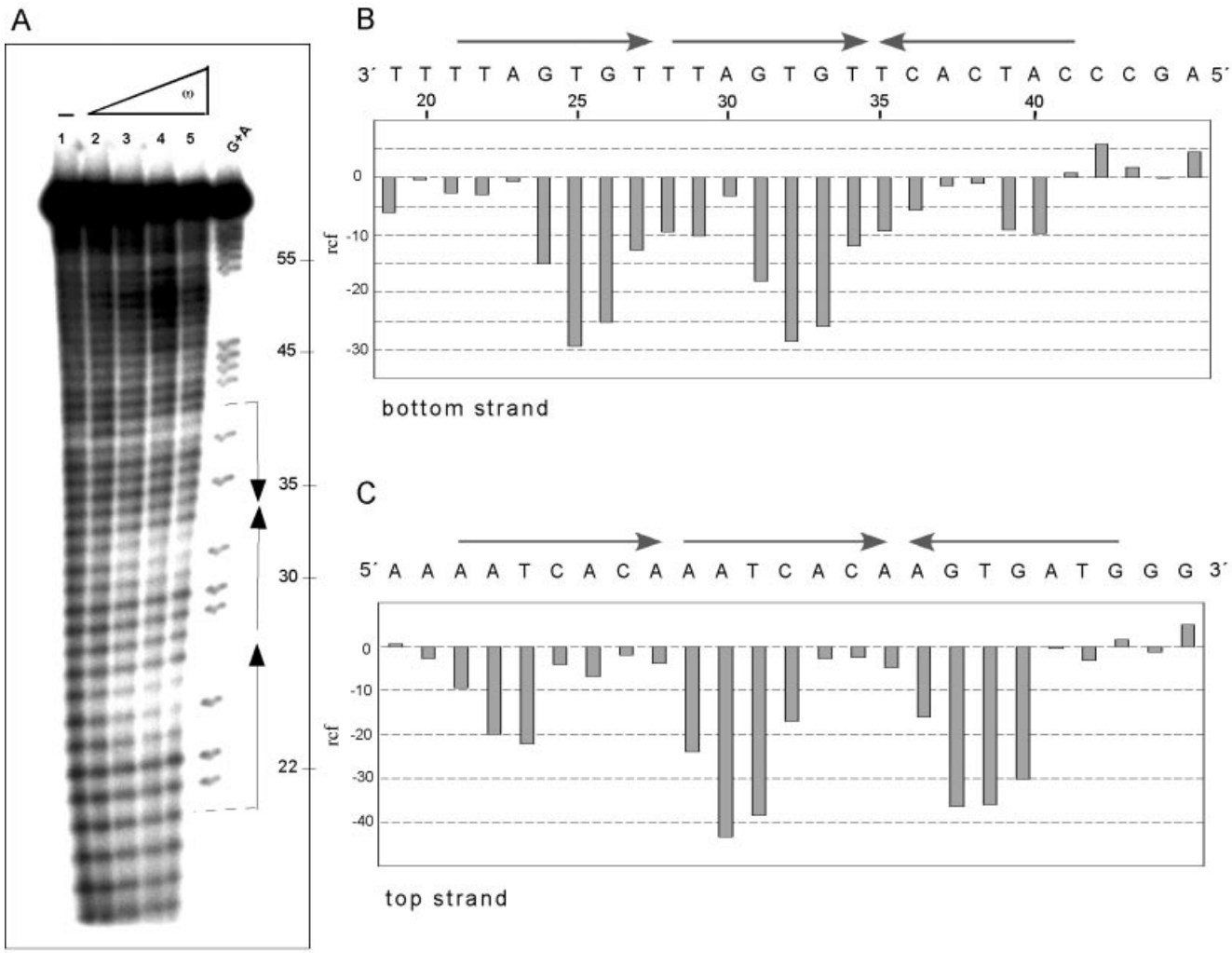

Figure 7. Hydroxyl radical footprinting of ω_2 protein bound to DNA with three heptads. The 66 bp [α-^{32}P]HindIII–KpnI [bottom strand (**A** and **B**)] or the 71 bp [α-^{32}P]EcoRI–SphI [top strand (**C**)] (2 nM) with three DNA heptads in $\longrightarrow_2\longleftarrow$ orientation, in the presence of 1 µg of poly[d(I-C)] as non-specific competitor DNA, was incubated and hydroxyl radical footprinted at ω_2 concentrations as described in Figure 6. The nucleotide sequence of $\longrightarrow_2\longleftarrow$ DNA and histograms of hydroxyl radical footprinting of bottom (B) and top (C) strands are shown. The relative cleavage frequency is shown as described in Figure 6.

He1318/17-1 and We1745/5-1 to H.W. and Sa196/38-1 to W.S. from the Deutsche Forschungsgemeinschaft and Fonds der Chemischen Industrie, and EU grant QLK3-CT-2001-00277 to J.C.A., H.W. and W.S. A.B. de la H. was recipient of a Fellowship of the Gobierno Vasco and F.P. was recipient of a Fellowship of the EU grant QLK3-CT-2001-00277.

REFERENCES

1. Ptashne,M. (1986) *A Genetic Switch. Gene Control and Phage Lambda*. Cell Press and Blackwell Scientific Publications, Cambridge, UK.
2. de la Hoz,A.B., Ayora,S., Sitkiewicz,I., Fernandez,S., Pankiewicz,R., Alonso,J.C. and Ceglowski,P. (2000) Plasmid copy-number control and better-than-random segregation genes of pSM19035 share a common regulator. *Proc. Natl Acad. Sci. USA*, **97**, 728–733.
3. Blanco,A.G., Sola,M., Gomis-Ruth,F.X. and Coll,M. (2002) Tandem DNA recognition by PhoB, a two-component signal transduction transcriptional activator. *Structure (Camb)*, **10**, 701–713.
4. Kalivoda,K.A., Steenbergen,S.M., Vimr,E.R. and Plumbridge,J. (2003) Regulation of sialic acid catabolism by the DNA binding protein NanR in *Escherichia coli*. *J. Bacteriol.*, **185**, 4806–4815.
5. Moller-Jensen,J., Borch,J., Dam,M., Jensen,R.B., Roepstorff,P. and Gerdes,K. (2003) Bacterial mitosis: ParM of plasmid R1 moves plasmid DNA by an actin-like insertional polymerization mechanism. *Mol. Cell*, **12**, 1477–1487.
6. Somers,W.S. and Phillips,S.E. (1992) Crystal structure of the met repressor-operator complex at 2.8 Å resolution reveals DNA recognition by β-strands. *Nature*, **359**, 387–393.
7. Raumann,B.E., Rould,M.A., Pabo,C.O. and Sauer,R.T. (1994) DNA recognition by β-sheets in the Arc repressor-operator crystal structure. *Nature*, **367**, 754–757.
8. Schildbach,J.F., Karzai,A.W., Raumann,B.E. and Sauer,R.T. (1999) Origins of DNA-binding specificity: role of protein contacts with the DNA backbone. *Proc. Natl Acad. Sci. USA*, **96**, 811–817.
9. Gomis-Ruth,F.X., Sola,M., Acebo,P., Parraga,A., Guasch,A., Eritja,R., Gonzalez,A., Espinosa,M., del Solar,G. and Coll,M. (1998) The structure of plasmid-encoded transcriptional repressor CopG unliganded and bound to its operator. *EMBO J.*, **17**, 7404–7415.
10. Murayama,K., Orth,P., de la Hoz,A.B., Alonso,J.C. and Saenger,W. (2001) Crystal structure of omega transcriptional repressor encoded by *Streptococcus pyogenes* plasmid pSM19035 at 1.5 Å resolution. *J. Mol. Biol.*, **314**, 789–796.
11. Golovanov,A.P., Barilla,D., Golovanova,M., Hayes,F. and Lian,L.Y. (2003) ParG, a protein required for active partition of bacterial plasmids,

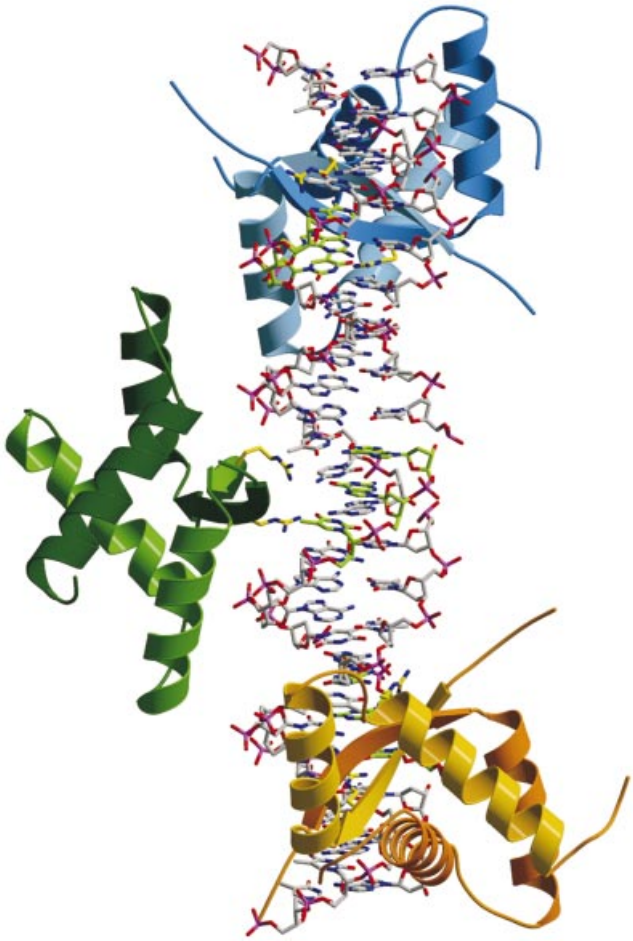

Figure 8. ω_2–DNA complex modeled on the basis of the MetJ–DNA complex. In the latter, two MetJ dimers bind to DNA tandem repeats and the entire lengths of α-helices A of adjacent MetJ are involved in cooperative MetJ–MetJ interactions (32). Ribbon representation of three ω_2 proteins [with secondary structure $(\beta\alpha A\alpha B)_2$] bound to a 25 bp straight B-DNA containing three heptads in direct orientation, $\longrightarrow_3$ with center-to-center distance 7 bp shown in stick form (5′-$^{A}/_{T}$ATCAC$^{A}/_{T}$-3′, the complementary 3′-AGT-5′ of the central 5′-TCA-3′ were denoted in green). The antiparallel N-terminal β-structure of ω_2 binds to the DNA operator half-site and is inserted in the major groove, with R31 and R31′ (their conformation in the complex is not known, indicated by yellow sticks) probably hydrogen bonding to guanine. The βαAαB subunits of each ω_2 are colored differently. The α-helices A of adjacent ω_2 are so close together that they could interact if the ω_2-bound heptads are bent or if ω_2 is slightly rotated on the DNA binding site. The ω_2 protein bound from seven (*Pω*) to 10 heptads (*Pcop*S, see Fig. 1) should wrap around the DNA helix.

has a dimeric ribbon-helix-helix structure. *Mol. Microbiol.*, **50**, 1141–1153.

12. Schreiter,E.R., Sintchak,M.D., Guo,Y., Chivers,P.T., Sauer,R.T. and Drennan,C.L. (2003) Crystal structure of the nickel-responsive transcription factor NikR. *Nature Struct. Biol.*, **10**, 794–799.
13. Camacho,A.G., Misselwitz,R., Behlke,J., Ayora,S., Welfle,K., Meinhart,A., Lara,B., Saenger,W., Welfle,H. and Alonso,J.C. (2002) *In vitro* and *in vivo* stability of the $\varepsilon_2\zeta_2$ protein complex of the broad host-range *Streptococcus pyogenes* pSM19035 addiction system. *Biol. Chem.*, **383**, 1701–1713.
14. Meinhart,A., Alonso,J.C., Strater,N. and Saenger,W. (2003) Crystal structure of the plasmid maintenance system ε/ζ: functional mechanism of toxin zeta and inactivation by $\varepsilon_2\zeta_2$complex formation. *Proc. Natl Acad. Sci. USA*, **100**, 1661–1666.
15. Rhodes,D. and Klug,A. (1986) An underlying repeat in some transcriptional control sequences corresponding to half a double helical turn of DNA. *Cell*, **46**, 123–132.
16. Xu,X., Sun,Y.L. and Hoey,T. (1996) Cooperative DNA binding and sequence-selective recognition conferred by the STAT amino-terminal domain. *Science*, **273**, 794–797.
17. Xiao,H., Perisic,O. and Lis,J.T. (1991) Cooperative binding of Drosophila heat shock factor to arrays of a conserved 5 bp unit. *Cell*, **64**, 585–593.
18. Uegaki,K., Shirakawa,M., Fujita,T., Taniguchi,T. and Kyogoku,Y. (1993) Characterization of the DNA binding domain of the mouse IRF-2 protein. *Protein Eng.*, **6**, 195–200.
19. Ou,X.M., Storring,J.M., Kushwaha,N. and Albert,P.R. (2001) Heterodimerization of mineralocorticoid and glucocorticoid receptors at a novel negative response element of the 5-HT1A receptor gene. *J. Biol. Chem.*, **276**, 14299–14307.
20. Umesono,K., Murakami,K.K., Thompson,C.C. and Evans,R.M. (1991) Direct repeats as selective response elements for the thyroid hormone, retinoic acid and vitamin D3 receptors. *Cell*, **65**, 1255–1266.
21. Naar,A.M., Boutin,J.M., Lipkin,S.M., Yu,V.C., Holloway,J.M., Glass,C.K. and Rosenfeld,M.G. (1991) The orientation and spacing of core DNA-binding motifs dictate selective transcriptional responses to three nuclear receptors. *Cell*, **65**, 1267–1279.
22. Rastinejad,F., Perlmann,T., Evans,R.M. and Sigler,P.B. (1995) Structural determinants of nuclear receptor assembly on DNA direct repeats. *Nature*, **375**, 203–211.
23. Studier,F.W. (1991) Use of bacteriophage T7 lysozyme to improve an inducible T7 expression system. *J. Mol. Biol.*, **219**, 37–44.
24. Sambrook,J., Fritsch,E.F. and Maniatis,T. (1989) *Molecular Cloning: A Laboratory Manual.* 2nd Edn. Cold Spring Harbor Laboratory Press, Cold Spring Harbor, NY.
25. Murayama,K., de la Hoz,A.B., Alings,C., Lopez,G., Orth,P., Alonso,J.C. and Saenger,W. (1999) Crystallization and preliminary X-ray diffraction studies of *Streptococcus pyogenes* plasmid pSM19035-encoded omega transcriptional repressor. *Acta. Crystallogr. D Biol. Crystallogr.*, **55**, 2041–2042.
26. Misselwitz,R., de la Hoz,A.B., Ayora,S., Welfle,K., Behlke,J., Murayama,K., Saenger,W., Alonso,J.C. and Welfle,H. (2001) Stability and DNA-binding properties of the omega regulator protein from the broad-host range *Streptococcus pyogenes* plasmid pSM19035. *FEBS Lett.*, **505**, 436–440.
27. Speck,C., Weigel,C. and Messer,W. (1999) ATP- and ADP-dnaA protein, a molecular switch in gene regulation. *EMBO J.*, **18**, 6169–6176.
28. Tullius,T.D. and Dombroski,B.A. (1986) Hydroxyl radical footprinting: high-resolution information about DNA-protein contacts and application to lambda repressor and Cro protein. *Proc. Natl Acad. Sci. USA*, **83**, 5469–5473.
29. Hammes,G.G. (2000) *Thermodynamics and Kinetics for the Biological Sciences*. Wiley-Interscience, New York, Chichester, Weinheim, Brisbane, Singapore, Toronto, Canada.
30. Smith,T.L. and Sauer,R.T. (1995) P22 Arc repressor: role of cooperativity in repression and binding to operators with altered half-site spacing. *J. Mol. Biol.*, **249**, 729–742.
31. Smith,T.L. and Sauer,R.T. (1996) Role of operator subsites in Arc repression. *J. Mol. Biol.*, **264**, 233–242.
32. Phillips,S.E., Manfield,I., Parsons,I., Davidson,B.E., Rafferty,J.B., Somers,W.S., Margarita,D., Cohen,G.N., Saint-Girons,I. and Stockley,P.G. (1989) Cooperative tandem binding of met repressor of *Escherichia coli*. *Nature*, **341**, 711–715.
33. Somers,W.S., Rafferty,J.B., Phillips,K., Strathdee,S., He,Y.Y., McNally,T., Manfield,I., Navratil,O., Old,I.G., Saint-Girons,I. *et al.* (1994) The Met repressor-operator complex: DNA recognition by β-strands. *Ann. N. Y. Acad. Sci.*, **726**, 105–117.
34. Dostál,L., Misselwitz,R., Laettig,S., Alonso,J.C. and Welfle,H. (2003) Raman spectroscopy of regulatory protein Omega from *Streptococcus pyogenes* plasmid pSM19035 and complexes with operator DNA. *Spectroscopy*, **17**, 435–445.